Quantitation of Small-Animal ^{124}I Activity Distributions Using a Clinical PET/CT Scanner

Dinko E. González Trotter, PhD[1]; Ravindra M. Manjeshwar, PhD[1]; Mohan Doss, PhD[2]; Calvin Shaller, BS[3]; Matthew K. Robinson, PhD[3]; Reeti Tandon, MS[4]; Gregory P. Adams, PhD[3]; and Lee P. Adler, MD[2]

[1]Functional Imaging Laboratory, General Electric Global Research, Niskayuna, New York; [2]Molecular Imaging Laboratory, Fox Chase Cancer Center, Philadelphia, Pennsylvania; [3]Department of Medical Oncology, Fox Chase Cancer Center, Philadelphia, Pennsylvania; and [4]Prediction Algorithms Center of Excellence Laboratory, General Electric Global Research, Bangalore, India

Time-dependent PET imaging can be an important tool in the assessment of radiotracer performance in murine models. We have performed a quantitative analysis of PET images of ^{124}I, acquired on a clinical PET system using a small-animal phantom. We then compared the recovered activity concentrations with the known activity concentration in the phantom spheres. The recovery coefficients found from the phantom data were applied to in vivo ^{124}I anti-HER2/*neu* C6.5 diabody PET data and compared with necropsy biodistribution data from the same tumor-bearing immunodeficient mouse. **Methods:** The small-animal phantom consisted of a 4 × 8 cm water-filled acrylic cylinder with hollow spheres filled with water ranging in volume from 0.0625 to 1.0 mL and activity concentration of 27 ± 2 kBq/mL. The background activity concentrations varied from 0 to 0.05 to 0.10 of the spheres. Data were acquired at 0, 5, and 10 cm from the scanner longitudinal axis. Recovery coefficients were theoretically calculated for spheres of different volume, background-to-target concentrations, and distance from the scanner's longitudinal axis. The theoretic recovery coefficients were applied to the maximum sphere activity concentration measured from the PET images, thus obtaining a recovered activity concentration to be compared with the known activity concentration of the spheres. **Results:** The mean recovered activity concentration for the phantom spheres was 25 ± 2 kBq/mL. The ^{124}I diabody PET image of a mouse with a tumor xenograft was then analyzed using the techniques described. The tumor percentage injected dose per gram estimated from the murine PET image (4.8 ± 0.4) compared well with those obtained from necropsy studies (5.1). **Conclusion:** This study indicates the feasibility of performing quantitative imaging on murine ^{124}I antibody fragment PET images using a large-bore clinical scanner, which enables high-throughput studies to evaluate the performance of PET tracers in a timely and cost-effective manner by imaging multiple animals simultaneously. Tracers deemed promising by this screening method can then be further evaluated using traditional necropsy studies. Our group is currently conducting time-dependent ^{124}I diabody PET and necropsy comparative studies with larger numbers of mice.

Key Words: ^{124}I; antibody; PET; quantitation; murine model

J Nucl Med 2004; 45:1237–1244

Advances in antibody engineering have facilitated the isolation of antibody fragments with very high affinity and specificity for antigens commonly overexpressed in human cancers (*1*). Antibody fragments labeled with an appropriate PET radioisotope may provide an effective means of detection of very small lesions by virtue of high target-to-background ratios coupled with adequate tumor activity concentration. By targeting the appropriate antigen, antibody PET imaging may also prove to be very effective in the assessment of tumor response to therapy since, in principle, the signal observed in a treated tumor will be proportional to the number of antigens present and to the number of tumor cells that have not been destroyed by therapy. This is in contrast to ^{18}F-FDG PET imaging, where the tumor signal may actually increase for some time after treatment due to inflammation (*2*) or modified tumor cell metabolism of FDG in response to stress (*3*). Furthermore, antibody PET may provide superior detection and response assessment of lesions within or near organs with relatively high concentrations of FDG, such as the brain, heart, bone marrow (after chemotherapy treatment), liver, and bladder.

Imaging tracers are usually tested in small animals before translation into the clinic. This is also true of antibody-based PET tracers. The time-dependent assessment of tumor-specific antibody distributions in small animals is currently done through necropsy-based biodistribution studies, where cohorts of animals are killed at various time points for evaluation of activity concentration in different tissues. A noninvasive method of measuring antibody distributions at different time points would be very desirable, allowing for the use of fewer animals per study and smaller quantities of antibody that may be expensive or difficult to produce. In addition, a noninvasive method may enable screening of various radiotracers before carrying out a detailed necropsy study. PET offers the possibility of carrying out noninvasive biodistribution studies by imaging the same group of live

Received Oct. 1, 2003; revision accepted Mar. 16, 2004.

For correspondence or reprints contact: Dinko E. González Trotter, PhD, Functional Imaging Laboratory, General Electric Global Research Center, KW-C1308, 1 Research Cir., Niskayuna NY 12309.

E-mail: trottedi@crd.ge.com

animals at several time points and assessing the concentration of radiolabeled antibody in different tissues in a manner that interferes minimally with an animal's normal biology. This task imposes on PET the quantitative requirement of determining the absolute concentration of radioisotope within small objects, such as xenograft tumors and internal organs of mice, which may be a fraction of a cubic centimeter in size. This presents a challenge for traditional clinical PET systems whose intrinsic resolution is ~5-mm full width at half maximum (FWHM) at best, resulting in severe blurring of small activity distributions and systematic errors in any direct measurements of concentration attempted from the PET image (*4*). On the other hand, a clinical PET scanner allows for the simultaneous scanning of several animals by virtue of its large field of view (FOV) (*5*), its data acquisition properties are well understood, and its septa provide an effective means of rejecting scatter and spurious γ-coincidences that are associated with the prompt γ-emissions of many long-lived PET radioisotopes that are suitable for antibody imaging.

^{124}I is a promising PET radionuclide for antibody imaging because of its favorable binding chemistry, long half-life (4.2 d), and rapid clearance from most tissues. On the other hand, ^{124}I has a positron emission probability per disintegration of only 23% (*6*) and a γ-ray emission probability of >90% per disintegration (*7*). A significant number of prompt γ-rays are emitted in cascade with positrons, which produce true photon coincidence detections that are spatially uncorrelated, resulting in a quasiuniform background in the emission sinogram (*8*). The mean positron energy of ^{124}I (819 keV) is significantly greater than that of ^{18}F (250 keV), which is expected to result in additional resolution degradation of the PET image. In this study, we assessed the quantitative accuracy of a model that can be used in the determination of activity concentration measurements of ^{124}I distributions that resembled those from murine models with xenograft tumors and imaged with ^{124}I-labeled diabodies using a clinical PET/CT scanner, with the aim of producing in vivo longitudinal biodistribution data of ^{124}I diabody PET tracers.

MATERIALS AND METHODS

Phantom

A custom-made phantom (Fig. 1) was constructed to emulate the approximate scatter and attenuation properties of a small animal. The phantom consisted of a hollow acrylic cylinder, 4 cm in inner diameter and 8 cm in length. Spheric inserts with nominal volumes (*V*) of 0.0625, 0.125, 0.250, 0.5, and 1.0 mL (Data Spectrum) were used. All spheres had an initial ^{124}I activity concentration of 27 ± 2 kBq/mL. This activity was chosen based on the expected tumor percentage injected dose per gram (%ID/g) for diabodies—about 1 %ID/g at 48 h after injection—an injected dose of ~3.7 MBq, and imaging at 12–48 h after injection. Higher phantom target concentrations would decrease the statistical noise per voxel in the image, leading to better precision without detrimental effects to image quality or quantitation, but we chose to be conservative in the target concentration estimate. The ^{124}I background activity was changed by adding activity to the water surrounding the spheric inserts. Background-to-target concentrations of 0.00, 0.05, and 0.10 were investigated, which are representative of the background-to-tumor ratios observed at various time points during diabody necropsy biodistribution studies.

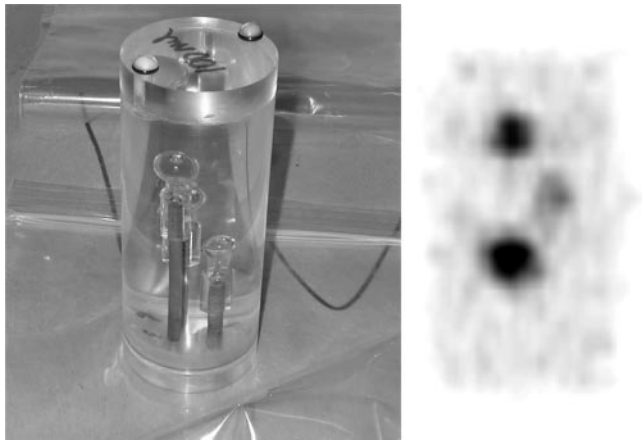

FIGURE 1. Picture of phantom with sphere inserts and corresponding coronal PET image with 0.05 background-to-target activity concentration ratios. The 0.25-mL (top), 0.125-mL (middle), and 0.0625-mL (bottom) spheres are clearly visible.

Measurement of Resolution Degradation Effect Due to ^{124}I Positron Range

The mean positron energy for ^{124}I is 819 keV, compared with 250 keV for ^{18}F. It is known that positrons from ^{124}I will, on average, annihilate at a greater distance from their point of origin than ^{18}F positrons (*7*). Line source data were acquired for ^{124}I and ^{18}F. A capillary glass tube of <1 mm in diameter was filled with activity and placed at the center of a water-filled Jaszczak phantom. The image was then reconstructed (*9*) using filtered backprojection (FBP) with a gaussian filter (7-mm FWHM cutoff). The 2-dimensional (2D) images were reconstructed with a pixel size of 0.53625 mm. The centroids of the capillary tube activity distribution of each image slice were made to align and then the slices were summed to reduce the noise for a better fit. Gaussians were fitted to profiles going through the center of the activity distributions. FWHM values were extracted from ^{18}F and ^{124}I measurements and their difference in quadrature was calculated to extract the degradation of the image point-spread function (PSF) due to positron range.

Phantom Data Acquisition and Reconstruction

PET measurements were performed on a Discovery LS PET/CT system (General Electric Medical Systems) operated in 2D high-sensitivity mode. The 14.9-cm-long axial FOV was sufficient to acquire the emission phantom data on a single 10-min bed position. Emission and transmission CT acquisitions were performed for the background-to-target ratio (b = 0, 0.05, 0.10), distance (d = 0, 5, 10 cm) from the z-axis of the scanner. Measurements at d = 0 cm were replicated 3 times to assess the repeatability of the activity concentration measurements. All images were reconstructed on a 256 × 256 × 35 grid (voxel size, 1.0725 × 1.0725 × 4.25 mm) using FBP with a gaussian postfilter cutoff set at 2-mm FWHM. The CT transmission images were automatically registered to the PET images by the scanner's built-in software, and attenuation correction maps were generated from the CT images

by thresholding and assigning the attenuation coefficient of water for 511-keV photons (0.0095 mm^{-1}) to the complete phantom and holder. No scatter correction or correction for prompt γ-emissions was necessary as they were determined to have negligible impact over the activity concentration of the phantom estimated from the PET images. The small mass of the phantom and holder provided little scatter, which was effectively rejected by the septa of the scanner and pulse-height discrimination, as were the prompt γ-emissions from ^{124}I (Fig. 2). This was determined by inspection of summed sinogram profiles, as done in (*8*). The scatter contribution was calculated using the Bergstrom model and the total contribution of scatter and prompt γ-rays to the region within the phantom was estimated at ~1% by a quadratic fit of the tails of the summed sinogram distribution.

Recovery Coefficients

A PET image is a representation of a distribution ρ of radionuclide based on the tomographic reconstruction from lines of response deduced from the detection of coincident photon events due to the annihilation of positrons with electrons. This representation is distorted in part by the count-limited nature of the data acquisition (statistical noise) and by resolution-degradation effects; such as annihilation photon noncollinearity, detector response function, and positron range. In the case of ^{124}I, positron range plays a significant role in resolution degradation.

The image $\tilde{\rho}$ (ignoring the contribution of noise, scatter, random, and prompt γ-events) corresponding to a 3-dimensional (3D) distribution of PET radionuclide ρ can be represented by:

$$\tilde{\rho} = S * R_{^{124}I} * G_{^{18}F} * \rho, \qquad \text{Eq. 1}$$

where $G_{^{18}F}$ is a 3D gaussian kernel representing the image blur due to the ^{18}F's annihilation photon noncollinearity, detector response function, and positron range. $R_{^{124}I}$ is a 3D gaussian kernel representing the additional degradation in resolution due to the positron range of ^{124}I, S is the filter applied to the reconstructed image and voxel discretization, and $*$ is the convolution operator. Assuming a homogeneous, spheric activity distribution of known volume V surrounded by a background of known constant activity concentration, it is possible to calculate recovery coefficients R, in a manner similar to (*10*), defined as:

$$R = \frac{\rho_{max}}{\tilde{\rho}_{max}}. \qquad \text{Eq. 2}$$

Recovery coefficients were calculated using Equation 2 for simulated spheric activity distributions with volumes, background-to-target ratios, and distances from the scanner's *z*-axis equal to those of the phantom measurements. The simulated distributions were then convolved with gaussian PSFs according to Equation 1. The measured maximum activity concentrations ρ_{max}^{exp} in the ^{124}I phantom spheres were multiplied by the appropriate recovery coefficient R to obtain the recovered activity concentration ρ_R. The recovered activity concentrations were then compared with the true activity concentration in the phantom spheres $\rho_{true} = 27 \pm 2$ kBq/mL.

The overall recovered concentration bias was estimated as the mean percentage difference for all recovered activity concentrations measured:

$$\%\bar{\Delta} = \frac{1}{N_d N_V N_b} \sum_d \sum_V \sum_b \%\Delta(d, V, b), \qquad \text{Eq. 3}$$

where

$$\%\Delta(d, V, b) = 100\,\frac{\rho_R(d, V, b) - \rho_{true}}{\rho_{true}}. \qquad \text{Eq. 4}$$

The SD from the percentage differences from each individual sphere measurement was given by:

$$\%\Delta_s = \left(\frac{1}{N_d N_V N_b - 1} \cdot \sum_d \sum_V \sum_b (\%\Delta(d, V, b) - \%\bar{\Delta})^2\right)^{1/2}. \qquad \text{Eq. 5}$$

A rough global estimate of the percent error bars on all PET concentration measurements was calculated from the average of all SDs of the activity concentration estimation of the three 10-min measurements of each sphere. This percentage error was scaled assuming Poisson statistics for different acquisition times. The distance d for each sphere was taken to be the same as the distance from the centroid of the phantom to the longitudinal axis of the scanner.

The individual impact of radial distance d, background-to-target ratio b, and sphere volume V parameters on the accuracy of the recovered activity ρ_R was assessed by taking the percent average error based on each parameter d, V, and b according to:

$$\Delta(d) = \frac{1}{N_V N_b} \sum_V \sum_b \%\Delta(d, V, b),$$

$$\Delta(V) = \frac{1}{N_d N_b} \sum_d \sum_b \%\Delta(d, V, b),$$

$$\Delta(b) = \frac{1}{N_V N_d} \sum_V \sum_d \%\Delta(d, V, b). \qquad \text{Eq. 6}$$

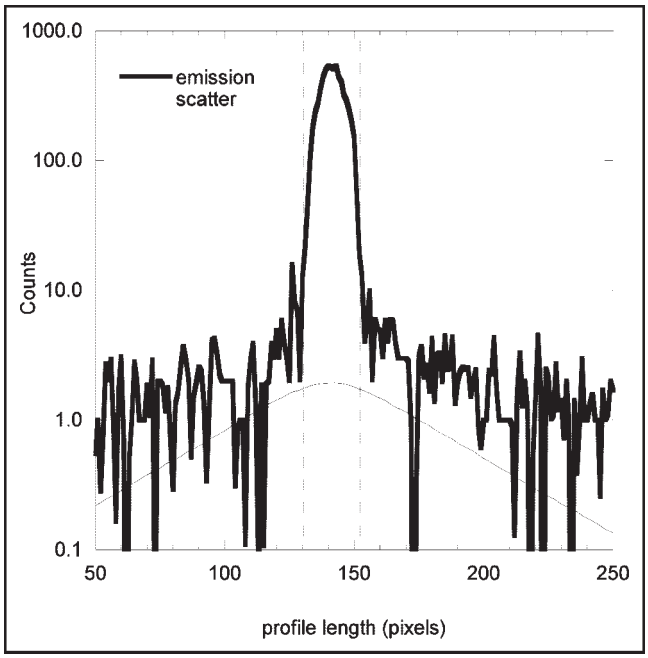

FIGURE 2. Profile for sinogram slice going through phantom (0.1 background-to-target activity concentration). Modest contribution of scatter and prompt γ-events is evident by small tails and low background counts outside of physical boundaries of the phantom itself (denoted by dashed vertical lines).

The uncertainty associated with each percent average error was calculated assuming a normal distribution and a 95% confidence interval.

C6.5 Diabody

Diabodies, noncovalently bound dimeric scFv constructs (molecular weight, ~52 kDa), have demonstrated especially promising biodistribution characteristics in preclinical experiments (*11*). In this study, the anti-HER2/*neu* (human epidermal growth factor receptor) diabody C6.5 was used in the in vivo PET acquisitions. This construct has an affinity ($\sim 4 \times 10^{-10}$ mol/L) for the HER2/*neu* antigen, which is overexpressed in close to 30% of human breast cancer cases, and overexpression is associated with a poor prognosis (*12*). In previous biodistribution studies, C6.5 has shown significant tumor accumulation (~6.5 %ID/g at 24 h after injection) (*13,14*). The diabody was expressed from TG1 *Escherichia coli* fully folded and purified by a 2-step process, immobilized metal-affinity chromatography, followed by size-exclusion chromatography on a Rainin Dynamax high-performance liquid chromatography (HPLC) system using a Superdex 75 column (Pharmacia), as previously described (*14*). The diabody was radiolabeled with ^{124}I using the IODO-BEADs method (Pierce). Briefly, 12 IODO-BEADs were washed in 100 mmol/L Tris, pH 6.5, for 5 min. ^{124}I (185 MBq) in 20 mmol/L NaOH (Advanced Nuclide Technologies, LLC) was neutralized by adding an equal volume of 2× saline (300 mmol/L) with 20 mmol/L HCl. The washed beads were transferred to a 17 × 100 mm tube along with the neutralized ^{124}I. After a 5-min incubation at room temperature, 5 mg of C6.5 diabody and 100 mmol/L Tris, pH 6.5, were added to the tube, and the mixture was incubated for 3 min with gentle mixing at room temperature. The reaction mixture was then chromatographed over a PD-10 size-exclusion column to remove unincorporated ^{124}I. Diabody was eluted with phosphate-buffered saline and collected in twenty 300-μL fractions. All radioactive fractions were assayed by instant thin-layer chromatography (ITLC) using silica ITLC strips (Biodex Medical Systems) and resolved using 10% trichloroacetic acid as a mobile phase. Fractions containing >99% protein-bound ^{124}I were pooled for use in imaging studies. The ability of the labeled protein to bind to the HER2 target antigen was assayed in a standard live-cell binding study as described (*15*).

Animal Imaging Study

A 6-wk-old inbred C.B17/Icr-*scid* mouse was obtained from the Fox Chase Cancer Center Laboratory Animal Facility. Approximately 2 mo before initiation of the biodistribution study, 3×10^6 SK-OV-3 cells were injected subcutaneously into the thigh of the mouse and a tumor xenograft was allowed to form.

^{124}I-Labeled C6.5 diabody (1.4 MBq) was administered by tail vein injection. The total injected dose was determined by counting the mouse on a Captus 600 thyroid scanner (Capintec). Whole-body counts and blood samples, collected by retroorbital bleeding, were obtained 10 min and 48 h after injection. At 48 h after injection, the mouse was anesthetized with tribromoethanol (Avertin; Winthrop Laboratories) and placed at the center of the FOV of the scanner; 3 sets of consecutive 10-min images were acquired (to prevent loss of all PET data in case the animal woke up or moved during scanning) and subsequently summed. Images were reconstructed and tumor activity concentration was quantitated using the same protocol as for the phantom acquisitions. The background activity concentration in the mouse was estimated from the mean value from a region of interest near the center of a transaxial slice adjacent to the tumor PET distribution. The percent error bars were assumed to be the same as those found in the phantom experiment. After imaging, the mouse was killed by CO_2 asphyxiation and dissected, the organs were weighed and counted for 1 min on a Cobra Quantum γ-counter (Packard Instruments), and the %ID/g tissue was calculated as previously described (*15*). The tumor imaged in this study was 0.67 g.

RESULTS

Positron Range Effect Measurements

Figure 3 shows the profiles across a line source for ^{124}I. The FWHMs extracted for ^{124}I and ^{18}F were $FWHM_{^{124}I} = 9.74$ mm and $FWHM_{^{18}F} = 8.71$ mm. Subtraction in quadrature yielded a difference in PSF FWHM due to the ^{124}I positron range of $\Delta_{^{124}I} = 4.4 \pm 1$ mm.

Recovery Coefficients and Quantitation of Phantom Spheres

The recovery coefficients calculated according to Equations 1 and 2 for the various sphere volumes V, background-to-target ratios b, and distance from the z-axis of the scanner d were applied to the experimental ^{124}I phantom data. Examples of the uncorrected ρ_{max}^{exp} and recovered ρ_R activity concentrations as a function of sphere size (V), position with respect to the z-axis (d), and background-to-target activity concentration (b) are shown in Figure 4. The mean recovered activity concentration for all sphere acquisitions was $\bar{\rho}_R = 24 \pm 2$ kBq/mL, in agreement with the true activity concentration $\rho_{true} = 27 \pm 2$ kBq/mL.

In Vivo Quantitation Results

The mouse injected with ^{124}I-labeled C6.5 diabody was imaged in the PET/CT (Fig. 5) scanner 48 h after injec-

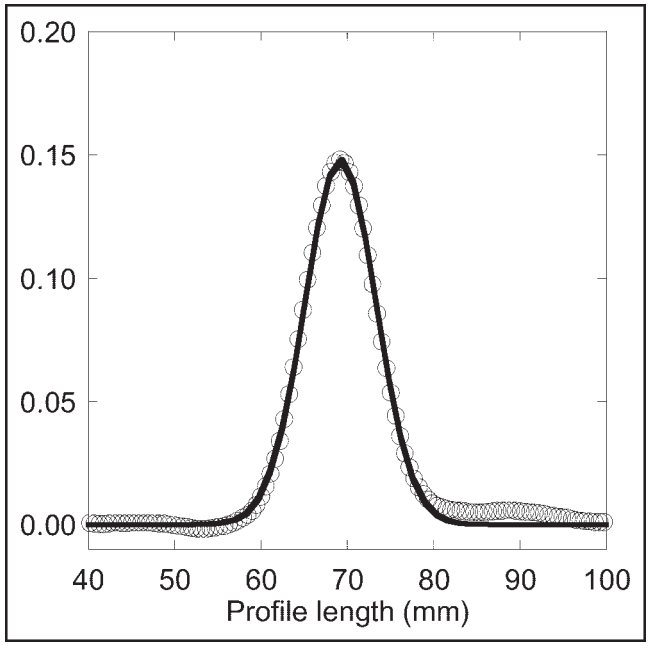

FIGURE 3. Profile across ^{124}I line source image fitted by a gaussian.

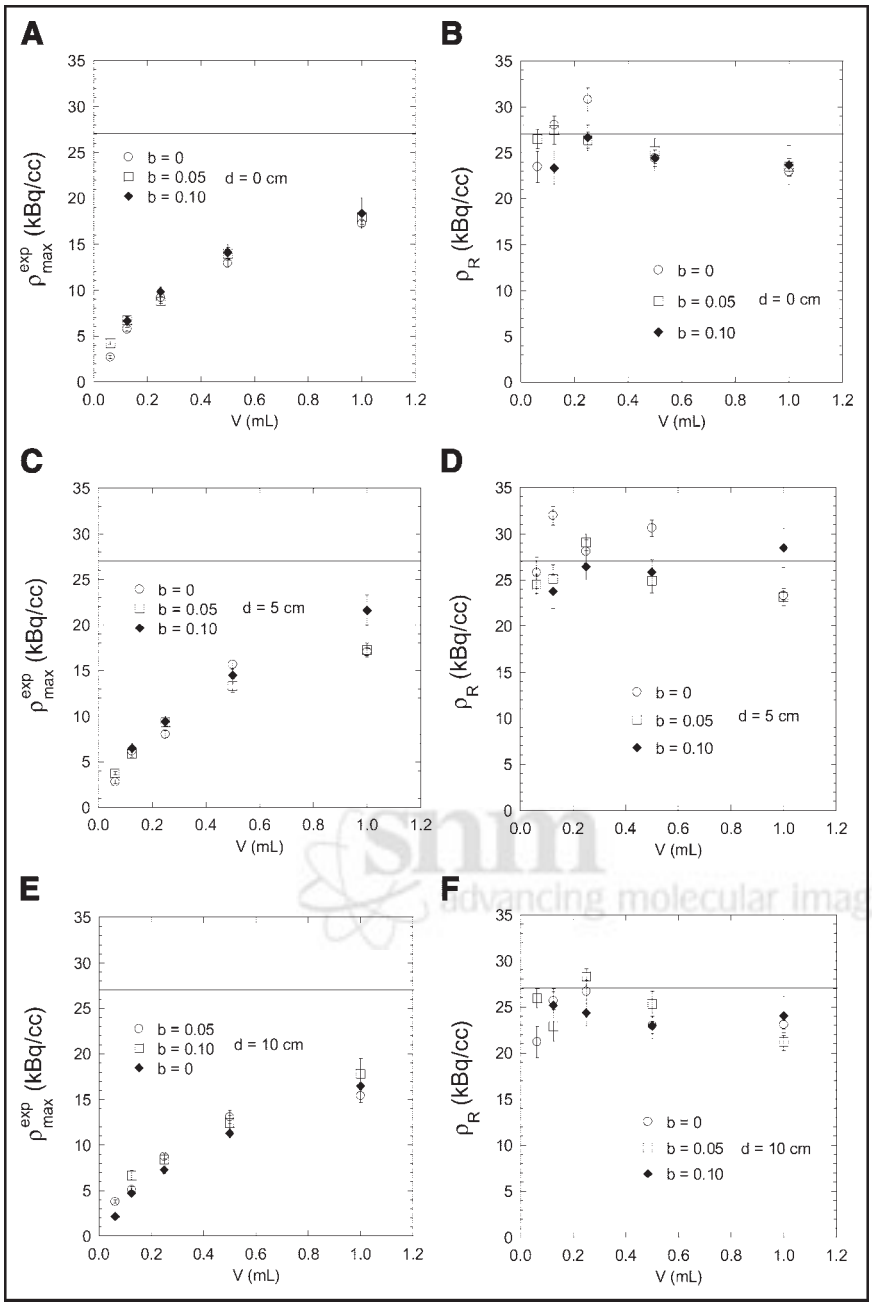

FIGURE 4. Maximum measured activity concentration (A, C, and E) and corresponding recovered activity concentration (B, D, and F) as function of sphere volume (V) for various background-to-target ratios and distances from *z*-axis of scanner. Horizontal line shows the ground-truth activity concentration in spheres.

tion and then immediately dissected for a necropsy-based biodistribution study. Figure 6 shows a coronal slice of the mouse PET image, with significant uptake in the tumor and the thyroid. The tumor activity concentration recovery coefficient was calculated based on tumor position in the scanner FOV, the tumor volume (measured after dissection), and the background activity present. The recovery coefficient was applied to the maximum activity concentration obtained from the tumor PET image. The %ID/g estimated from the PET image was 4.8 ± 0.4. The tumor %ID/g obtained from the necropsy biodistribution was 5.1.

DISCUSSION

^{124}I is a promising radionuclide for use in antibody PET imaging due to its chemical properties and relatively long half-life of 4.2 d. The present phantom study was aimed at assessing the potential of extracting accurate tumor activity concentration information from PET images of ^{124}I activity distributions similar to those found in murine antibody PET studies. In principle, the ability to quantitate PET images is limited by the intrinsic resolution of the PET scanner, the PSF degradation due to the relatively long positron range of ^{124}I, and the prompt γ-rays emitted in coincidence with positrons. Due to the compact activity distributions and

FIGURE 5. Mouse positioned on custom platform in Discovery LS PET/CT scanner.

small mass of the phantom used in this study, there was little scatter signal in the PET image. Most prompt γ-events associated with positron emission are rejected by the scanner's septa. The few prompt γ-events that register are assigned quasiuniformly throughout the FOV of the scanner, resulting in a very low signal per voxel compared with true coincidences (Fig. 2). This would not be the case if the ^{124}I source were comparable in size to the FOV of the scanner (such as in the case of a human patient).

In the case of multiple imaging of mice, the effect of scatter would be very small compared with the total signal. In 2D high-sensitivity mode, and using a National Electrical Manufacturers Association (NEMA) 2001 image-quality phantom on the standard patient bed, the scatter contribution is in the order of ~15% of the total signal. The volume of such a phantom is roughly 10,000 mL of water-equivalent material compared with ~9 mice imaged simultaneously, which amount to ~225 mL of water-equivalent material. Furthermore, mice can be positioned in an axially staggered fashion taking advantage of the large axial FOV of the scanner, which is about 15 cm, so the chances of scatter from one mouse to another are minimized. From the point of view of scatter, mice really behave like very compact sources distributed throughout the larger FOV of the scanner, and not so much as an extended source that is close in size to the FOV (as a patient with actual background activity would). The holder for the mice can be made of very light material (polystyrene or thin-walled acrylic) so the scatter contribution from the holder is negligible. If one assumes that the scatter signal in 2D high-sensitivity mode roughly scales with volume in a given image slice, 9 mice amount to about 70 cm^3 and the NEMA phantom amounts to ~470 mL, so the scatter signal from the mice will be about 15% that of the NEMA phantom, or 2% of the total signal. If mice are axially staggered, then the effect of scatter will be even smaller. Likewise, the impact of the prompt γ-rays will be very small: In 2D high-sensitivity mode, prompt γ-rays from ^{124}I (as with other isotopes such as ^{86}Y (*8*)) present a quasiuniform background throughout the FOV of the image. Our single-phantom measurements indicate that the prompt γ-background (concentration) amounts to about 0.2% of the signal from the phantom (from the extreme of the sinogram distribution tails). As more sources of similar strength are added, the signal from the prompt γ-rays should go up linearly, so 9 such phantoms (or mice) would produce a bias of about 2%, also quite small compared with the total true events detected. Once again, if mice are axially staggered, then the prompt γ-contribution for a given image slice will be even smaller. If the effects of scatter and prompt γ-rays turned out not to be as small as predicted, one could apply the prompt correction techniques developed by Pentlow et al. (*8*), coupled with standard scatter-correction techniques based on convolution or tail-fitting.

^{124}I has a significantly higher positron energy spectrum than ^{18}F. Our measurements indicated a PSF degradation of ^{124}I PET images compared with ^{18}F somewhat smaller than that found by Pentlow et al. (*7*). We used a linear gaussian model to estimate the PSF degradation due to the ^{124}I positron range. The gaussian model was applied to the calculation of recovery coefficients for spheric ^{124}I distributions. The theoretic recovery coefficients R were used in the correction of experimental phantom data (Fig. 4), leading to a bias and SD of −7% and 7%, respectively, with respect to the true activity concentration in the spheres (Eqs. 3–5). The impact of the variables d, V, and b on the accuracy of the recovered activity concentration is shown in the plot of the percent average errors based on Equation 6 (Fig. 7). The recovered activity is underestimated between ~4% and ~12% for all variables. Regression analysis showed that, aside from the global negative bias, the percent average errors shows a slight dependence on V; there was no dependence on b. The effect of radial distance d is somewhat more

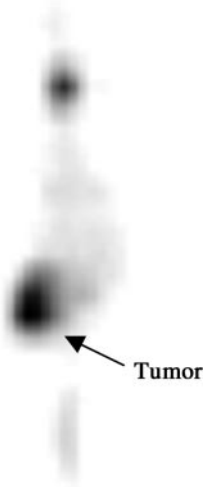

FIGURE 6. PET image of mouse 48 h after injection.

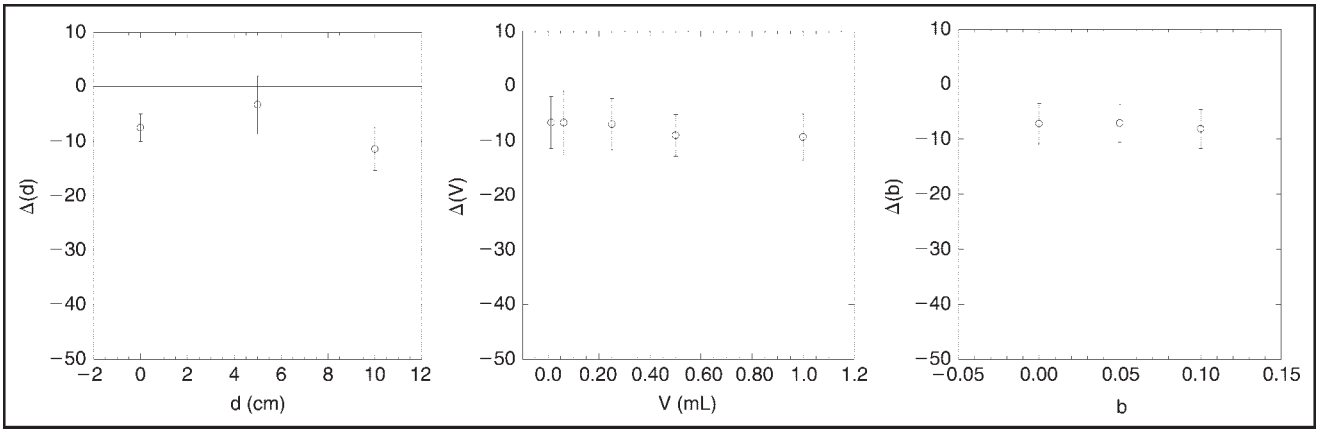

FIGURE 7. Plots of percent average error of recovered activity concentration based on radial distance *d*, sphere volume *V*, and background-to-target ratio *b*.

pronounced and suggests a quadratic dependency. The sources of discrepancy may come from an inaccurate (simple gaussian) description of the PSF degradation due to ^{124}I. The accuracy of the recovery coefficients may be improved by the incorporation of a more realistic positron-range spread function—which is known to be more heavy-tailed than a gaussian for many PET isotopes with positron energy spectra that are more energetic than that of ^{18}F (*8,16*). Alternatively, a direct empiric approach could be used, where recovery coefficients are obtained directly from high-count phantom data for different PET isotopes.

The tumor %ID/g was calculated from a murine PET image using ^{124}I-labeled anti-HER2/*neu* diabody C6.5. In this case, tumor activity concentrations from quantitated tumor PET and necropsy biodistribution data were compared and found to agree within experimental error. Underlying assumptions of the model are spheric tumor shape and homogeneous distribution of activity throughout the tumor and background. The recovery coefficients require tumor volume information, which, in our case, was derived from postmortem tumor mass measurement, assuming a tumor density of 1 g/cm^3. Longitudinal studies taking place for more than several days—depending on the tumor model—would imply significant changes to the tumor volume and, in this case, an endpoint tumor volume assessment would not be adequate for the quantitation of PET images acquired at a time much earlier than when the animal is killed. This problem may be solved by the use of anatomic imaging modalities such as CT and MRI, which may provide tumor volume information very near the time of the PET scan. In the case of the clinical PET/CT system used in this study, standard acquisition techniques did not allow sufficient soft-tissue contrast to permit an accurate assessment of tumor volume. Further exploration of other acquisition techniques, or the use of MRI or dedicated small-animal CT, may provide a noninvasive solution to accurate tumor volume measurement in mice. The good agreement between the ^{124}I anti-HER2/*neu* biodistribution and PET tumor concentrations suggest that the previous assumptions are reasonable for this particular ^{124}I diabody and tumor model. If compensation for the bias in the theoretic recovery coefficient is included, then the tumor concentration from PET increases to 5.3 ± 0.4 %ID/g, in better agreement with the necropsy result of 5.1 %ID/g. Without the use of a recovery coefficient, the activity concentration in the tumor would have been underestimated by 35%. Smaller tumors would make the bias even more pronounced if recovery coefficients are not used.

Deviation of tumor geometry from a spheric geometry has a nonnegligible effect on the recovery coefficient. Tumor geometry information derived from the endpoint necropsy, from the PET image itself, or from CT or MRI may be incorporated in the calculation of recovery coefficients and lead to further improvement in the accuracy of the recovered tumor activity concentration. Xenograft tumors are typically located on the flank or leg of the animal. The resulting inhomogeneity of the background activity surrounding the tumor will have an impact on tumor PET concentration measurements. Incorporation of background variability in the calculation of recovery coefficients should lead to improved accuracy of tumor activity concentration measurements from PET images. Quantitation of organs with major radiotracer uptake is important for a complete and meaningful biodistribution assessment. Our group is currently conducting a more extensive study to look into the correlation of PET and necropsy-based biodistribution data for organs in murine models.

The PET quantitation techniques investigated here can be extended in a straightforward manner to other PET isotopes with positron ranges longer than that of ^{18}F and that are suitable for antibody labeling due to their half-life, such as ^{76}Br (16.2 h), ^{86}Y (14.7 h), and ^{55}Co (17.5 h).

CONCLUSION

Necropsy-based biodistribution studies of radiolabeled ligands are usually performed by killing cohorts of animals at various time points after injection, to measure the average

activity concentration in organs or tissues of interest. We present a method of quantitative evaluation of radiolabeled antibodies using a clinical PET scanner that may be an attractive option since it would permit simultaneous noninvasive time-dependent biodistribution studies of the same group of animals. The present phantom and small-animal measurements suggest that useful in vivo biodistribution information may be recovered from murine PET images acquired on a clinical PET scanner. Quantitative murine PET imaging using a clinical scanner may allow faster screening of radiolabeled ligands, with subsequent detailed necropsy studies for those agents that show the most promise. A large-bore clinical scanner offers the possibility of simultaneous imaging and absolute quantitation of tracer uptake for several small animals in a single bed position and increased throughput for the evaluation of PET tracers in vivo, which may be of utility in the preclinical evaluation of novel PET ligands.

ACKNOWLEDGMENTS

The authors thank Richard F. Schneider for help with phantom preparation and Steven Kohlmyer for scanner PSF data.

REFERENCES

1. Adams GP. Improving the tumor specificity and retention of antibody-based molecules. *In Vivo.* 1998;12:11–22.
2. Jager PL, Vaalburg W, Pruim J, de Vries EGE, Langen K-J, Piers DA. Radiolabeled amino acids: basic aspects and clinical applications in oncology. *J Nucl Med.* 2001;42:432–445.
3. Smith TAD, Maisey NR, Titley JC, Jackson LE, Leach MO, Ronen SM. Treatment of SW620 cells with Tomudex and oxaliplatin induces changes in 2-deoxy-D-glucose incorporation associated with modifications in glucose transport. *J Nucl Med.* 2000;41:1753–1759.
4. Chen C-H, Muzic RF Jr, Nelson AD, Adler LP. Simultaneous recovery of size and radioactivity concentration of small spheroids with PET data. *J Nucl Med.* 1999;40:118–130.
5. Lövqvist A, Humm JL, Sheikh A, et al. PET imaging of ^{86}Y-labeled anti-Lewis Y monoclonal antibodies in a nude mouse model: comparison between ^{86}Y and ^{111}In radiolabels. *J Nucl Med.* 2001;42:1281–1287.
6. Laforest R, Douglas DJ, Welch MJ. MicroPET imaging with nonconventional isotopes. *IEEE Trans Nucl Sci.* 2002;49:2119–2126.
7. Pentlow KS, Graham MC, Lambrecht RM, Cheung N-KV, Larson SM. Quantitative imaging of I-124 using positron emission tomography with application to radioimmunodiagnosis and radioimmunotherapy. *Med Phys.* 1991;18:357–366.
8. Pentlow KS, Finn RD, Larson SM, Erdi YE, Beattie BJ, Humm JL. Quantitative imaging of yttrium-86 with PET: the occurrence and correction of anomalous apparent activity in high density regions. *Clin Positron Imaging.* 2000;3:85–90.
9. Fessler JA. *ASPIRE 3.0 User's Guide: A Sparse Iterative Reconstruction Library*. Technical Report 293. Communication and Signal Processing Laboratory, Department of Electrical Engineering and Computer Science, University of Michigan, Ann Arbor, MI; July 1995.
10. Kessler RM, Ellis JR Jr, Eden M. Analysis of emission tomographic scan data: limitations imposed by resolution and background. *J Comput Assist Tomogr.* 1984;8:514–522.
11. Pavlinkova G, Beresford GW, Booth BJM, Batra SK, Colcher D. Pharmacokinetics and biodistribution of engineered single-chain antibody constructs of Mab CC49 in colon carcinoma xenografts. *J Nucl Med.* 1999;40:1536–1546.
12. Slamon DJ, Clark GM, Wong SG, Levin WJ, Ullrich A, McGuire WL. Human breast cancer: correlation of relapse and survival with amplification of the HER-2/neu oncogene. *Science.* 1987;235:177–182.
13. Nielsen UB, Adams GP, Weiner LM, Marks JD. Targeting of bivalent anti-ErbB2 diabody antibody fragments to tumor cells is independent of the intrinsic antibody affinity. *Cancer Res.* 2000;60:6434–6440.
14. Adams GP, Schier R, McCall AM, et al. Prolonged in vivo tumor retention of a human diabody targeting the extracellular domain of human HER2/neu. *Br J Cancer.* 1998;77:1405–1412.
15. Adams GP, McCartney JE, Tai M-S, Oppermann H, et al. Highly specific in vivo tumor targeting by monovalent and divalent forms of 741F8 anti-C-Erbb-2 single-chain Fv. *Cancer Res.* 1993;53:4026–4034.
16. Levin CS, Hoffman EJ. Calculation of positron range and its effect on the fundamental limit of positron emission tomography system spatial resolution. *Phys Med Biol.* 1999;44:781–799.